

## Charge collective modes and dynamic pairing in the three-band Hubbard model. II. Strong-coupling limit

R. Raimondi, C. Castellani, and M. Grilli

*Dipartimento di Fisica, Università La Sapienza, Piazzale Aldo Moro, 00185 Roma, Italy*

Yunkyu Bang\* and G. Kotliar

*Serin Physics Laboratory, Rutgers University, Piscataway, New Jersey 08855-0849*

(Received 4 May 1992)

We analyze the dynamics of the charge degrees of freedom in the extended Hubbard model for the  $\text{CuO}_2$  planes in copper oxides in the strong-coupling limit. We analyze the behavior of the collective modes near the charge-transfer instability (CTI). The CTI is driven by an overdamped zero-sound mode when the Landau stability criterion  $F_0^s > -1$  is violated due to the charge-transfer mode-mediated attraction. The divergence of the compressibility at the CTI requires a Maxwell construction, which determines a region of phase separation. Near the phase-separation boundary, at intermediate doping, the singlet Cooper coupling is attractive both in the  $s$ - and  $d$ -wave channels. In the strong-coupling limit the excitonic energy  $\omega_{\text{exc}}$  is large and the energy scale for pairing is the Fermi energy itself.

### I. INTRODUCTION

In the preceding paper we described the interplay of the collective modes and the charge-transfer instability (CTI) in the extended Hubbard model in the weak-coupling limit. We found that the zero sound and the CT excitonic mode interplay to drive the instabilities and the superconducting pairing near phase separation. The weak-coupling approach probably gives qualitatively correct results for the intermediate to large doping region where the correlation effect is not strong. But in the copper oxides,  $U_d$  is larger than the bandwidth and the strong correlation effect is important anyway, especially close to half-filling. Moreover, the fact that some important results obtained in the weak-coupling framework (e. g.,  $s$ -wave pairing) are very sensitive to the strength of  $U_d$  motivates us to investigate the infinite  $U_d$  limit using the slave boson approach.

The recent analysis reported in Refs. 1 and 2 employed a large- $N$  technique combined with a slave boson technique to study the  $U_d = \infty$  limit of the three-band extended Hubbard model. According to that analysis, the CTI, together with phase separation, is present in the  $U_d = \infty$  limit just as in the weak-coupling limit. Furthermore,  $s$ - and  $d$ -wave pairings were found in the proximity of the phase separation. Therefore, regardless of the strength of  $U_d$ , a  $V$  of the same order of magnitude of  $t_{pd}$  is enough to give a CTI in the three-band extended Hubbard model. Moreover, this instability is intimately related to the phase separation and to the superconductivity.

However, there are several differences between the  $U_d = \infty$  limit and the weak-coupling limit. First, the strong-coupling technique is able to describe the metal-charge-transfer-insulator (MCTI) transition at the half-filling ( $\delta=0$ ), whereas the weak-coupling Hartree-Fock approximation cannot describe the insulating regime.<sup>3</sup>

This fact is reflected in a different location of the phase-separation region in the phase diagram. While in the weak-coupling case<sup>4</sup> the phase separation and the concomitant instabilities are approached as one increases doping, in the strong-coupling case<sup>1,2</sup> those features occur for small doping in the proximity of the MCTI transition. In both cases the physical reason for the phase separation is the decrease of the renormalized kinetic-energy contribution to the total energy. Roughly speaking phase separation appears when the renormalized kinetic energy is no longer large enough to provide an upward curvature to the total energy as a function of doping. In the weak-coupling limit decreasing doping stabilizes the system, since the renormalized kinetic energy roughly behaves like the unrenormalized kinetic energy, which has the largest upward curvature at half filling. This is not the case in the strong-coupling limit since the renormalized bandwidth goes to zero near the insulating phase and phase separation first appears near zero doping by increasing  $V$ .

A second difference between weak- and strong-coupling limits is that the excitonic collective mode has, in general, a high energy in the strong-coupling limit, even in the proximity of the CTI. Nevertheless, as in the weak-coupling theory, this mode plays an important role to induce the CTI, the phase separation, and the superconductivity.

In order to shed light on these aspects, in the next sections we extend the work of Refs. 1 and 2 to the dynamic limit. We first introduce the strong-coupling formalism and review the mean-field analysis. Then we analyze the collective modes at small doping close to the insulating phase, where an analytical treatment is feasible. The instabilities are then considered in the context of the Fermi-liquid theory. Finally numerical results are presented.

## II. STRONG-COUPPLING FORMALISM

### A. Static mean-field analysis: An overview

In the  $U_d = \infty$  limit of model (1) in the companion paper a no double occupancy constraint arises on copper sites  $\sum_{\sigma} d_{i\sigma}^{\dagger} d_{i\sigma} \leq 1$  containing the major difficulty of the formal treatment. A standard trick to handle the constraint is the slave boson technique,<sup>5</sup> transforming the inequality into a completeness relation. The introduction of bosonic degrees of freedom “labeling” the empty sites results in the mapping

$$d_{i\sigma}^{\dagger} \rightarrow d_{i\sigma}^{\dagger} b_i, \quad d_{i\sigma} \rightarrow b_i^{\dagger} d_{i\sigma}. \quad (1)$$

Since a given copper site can only be either singly occupied by a fermion or singly occupied by an “emptiness” boson, the constraint assumes the form  $\sum_{\sigma} d_{i\sigma}^{\dagger} d_{i\sigma} + b_i^{\dagger} b_i = 1$ .

To avoid any perturbative approach in the coupling constants we provide the model of a small expansion parameter by means of a large- $N$  expansion technique assuming the spin index to run from 1 to  $N$ . In order to keep all the terms in the Hamiltonian of the same order  $N$ , the following rescaling of the couplings has to be per-

formed:

$$t_{pd} \rightarrow \frac{t_{pd}}{\sqrt{N}}, \quad V \rightarrow \frac{V}{N}.$$

Then the model is further modified by partially relaxing the constraint, which becomes  $\sum_{\sigma} d_{i\sigma}^{\dagger} d_{i\sigma} + b_i^{\dagger} b_i = q_0 N$ , with  $q_0 = \frac{1}{2}$  and  $N$  large. The original model can then be recovered by setting  $N=2$ .

On the other hand, the nearest-neighbor interaction term

$$\frac{V}{N} \sum_{ij\sigma\sigma'} n_{d_{i\sigma}} n_{p_{j\sigma'}} = \frac{V}{2N} \sum_{ij\sigma\sigma'} (n_{d_{i\sigma}} + \frac{1}{2} n_{p_{j\sigma'}})^2 - (n_{d_{i\sigma}} - \frac{1}{2} n_{p_{j\sigma'}})^2 \quad (2)$$

(here  $j$  labels the four oxygen sites surrounding the copper site  $i$ ) can be decoupled by means of a Hubbard-Stratonovich transformation by introducing two real fields  $X$  and  $Y$  coupled to the CT density  $n_d - n_p$  and to the total-charge density  $n_d + n_p$ , respectively (each density is taken per unit cell and per spin).<sup>6</sup>

The partition function of this system can then be written as a functional integral

$$Z = \int Dp_{\alpha\sigma}^{\dagger} Dp_{\alpha\sigma} Dd_{\sigma}^{\dagger} Dd_{\sigma} Db^{\dagger} Db D\lambda DX DY \exp \left[ - \int_0^{\beta} S d\tau \right], \quad (3)$$

$$S = \sum_i \left[ \sum_{\sigma} d_{i\sigma}^{\dagger} \frac{\partial d_{i\sigma}}{\partial \tau} + \sum_{\sigma\alpha=x,y} p_{i\sigma\alpha}^{\dagger} \frac{\partial p_{i\sigma\alpha}}{\partial \tau} + b_i^{\dagger} \frac{\partial b_i}{\partial \tau} \right] + \sum_i \left[ i\lambda_i (b_i^{\dagger} b_i - q_0 N) + \frac{N}{2V} (X_i^2 + Y_i^2) \right] + H, \quad (4)$$

$$H = \sum_{i,\sigma} d_{i\sigma}^{\dagger} d_{i\sigma} (\varepsilon_d^0 + i\lambda_i + X_i + iY_i) - \frac{1}{2} \sum_{i,\sigma,\alpha=\pm x,\pm y} p_{i\sigma\alpha}^{\dagger} p_{i\sigma\alpha} (X_i - iY_i) + \varepsilon_p^0 \sum_{i,\sigma,\alpha=x,y} p_{i\sigma\alpha}^{\dagger} p_{i\sigma\alpha} - \frac{t_{pd}}{\sqrt{N}} \sum_{i,\sigma} [(p_{i\sigma x}^{\dagger} - p_{i\sigma-x}^{\dagger} + p_{i\sigma y}^{\dagger} - p_{i\sigma-y}^{\dagger}) d_{i\sigma} b_i^{\dagger} + \text{c.c.}] - t_{pp} \sum_{i\sigma} [p_{i+x\sigma}^{\dagger} (p_{i\sigma-y} - p_{i\sigma y} + p_{i+2x\sigma y} - p_{i+2x\sigma-y}) + \text{c.c.}] . \quad (5)$$

In terms of the functional integral the large- $N$  expansion is a saddle-point expansion, the saddle-point mean-field solution being exact in the  $N = \infty$  limit.

The limitations of the present technique are due to the unknown convergency properties of the  $1/N$  expansion.

Another important limitation is given by the absence of magnetic phases in our treatment. Actually an effective magnetic coupling (like the superexchange  $J$  between copper spins) is, in principle, present in the model arising from a double exchange of bosons.<sup>7</sup> This process, however, turns out to be higher order in  $1/N$  (see the next subsection) so that, at the mean-field level and  $1/N$  corrections, the present description does not include relevant magnetic effects like long-range antiferromagnetic order and spiral spin phases. On the other hand, this approach has the advantage of being systematic in the derivation of higher-order corrections and of being non-perturbative in the physical couplings  $U_d$ ,  $\varepsilon_p^0 - \varepsilon_d^0$ , and  $t_{pd}$

so that all the various regimes of bare parameters can be explored.

Besides the above technical advantages the slave boson large- $N$  technique presents the physical advantage that its very starting point already contains some important physics, which is intrinsic of the large- $N$  version of the three-band extended Hubbard model and it is not introduced by any approximation (the mean-field solution being exact in the infinite- $N$  limit). Specifically it is able to describe already at the mean-field level the occurrence of a CT insulating phase at half filling.<sup>8</sup> For  $t_{pp}=0$  this happens when  $\varepsilon_p^0 - \varepsilon_d^0 + V > 3.34 t_{pd}$ . Of course, in this regime magnetism plays a major role in real systems, but it is important to recognize that the present model, intentionally designed to make evident the behavior of the charge degrees of freedom only, still captures the CT insulating character of the half-filled phase. The kinetic-energy reduction in the metallic phase due to the close-

ness to an insulating phase can indeed have important physical consequences.

The model (3)–(5) can be solved at the mean-field level (large  $N$ ) by setting the bosonic fields to uniform time-independent numbers  $\langle b_i \rangle = b_0 = \sqrt{N} r_0$ ,  $\langle \lambda_i \rangle = -i\lambda_0$ ,  $\langle X_i \rangle = X_0$ , and  $\langle Y_i \rangle = -iY_0$ . Notice that the paths for  $\lambda_i$  and  $Y_i$  in the functional integral have been deformed from the real axis inside the complex plane to meet the saddle-point solutions. At this point the model has become a tight-binding model for free fermions describing the coherent motion of the quasiparticles of a Fermi liquid. The only effect of the interactions is in the renormalization of the tight-binding parameters:  $r_0$  multiplicatively renormalizes the hopping  $t_{pd}$  leading to a reduction of the quasiparticle bandwidth, whereas  $\lambda_0$ ,  $X_0$ , and  $Y_0$  shift the bare atomic levels

$$\varepsilon_p = \varepsilon_p^0 - (X_0 - Y_0),$$

$$\varepsilon_d = \varepsilon_d^0 + (X_0 + Y_0) + \lambda_0.$$

The mean-field values of the fields must be self-consistently determined by solving the integral equations arising from the stationary conditions of the free-energy functional per site and per spin

$$F = \lambda_0(r_0^2 - q_0) + \frac{1}{V}(X_0^2 - Y_0^2) - \frac{T}{N_s} \sum_{k,l} \ln[1 + e^{-\beta[E_l(k) - \mu]}]. \quad (6)$$

$E_l(k)$  are the three eigenvalues of the tight-binding Hamiltonian (5) renormalized by the saddle-point values of the bosonic fields. The self-consistency equations must be solved together with the equation for the chemical potential fixing to  $(1+\delta)q_0$  the average particle number per cell and per spin.

The whole set of equations is given by

$$\frac{\partial F}{\partial W} = \sum_{k,l,i,j} f[E_l(k) - \mu] U_{li}(k) \left[ \frac{\partial H}{\partial W} \right]_{ij} U_{jl}^\dagger(k) = 0,$$

$$-\frac{\partial F}{\partial \mu} = \sum_{kl} f[E_l(k) - \mu] = (1+\delta)q_0,$$

where  $W$  indicates the mean-field parameters (i.e.,  $r_0$ ,  $\lambda_0$ ,  $X_0$ , and  $Y_0$ ), the  $U$ 's are the matrices which diagonalize the Hamiltonian at a given point in  $k$  space, and  $f(E)$  is the Fermi function.

In the particular case  $t_{pp} = 0$  the renormalized band structure assumes a simple form

$$E_1(k) = \frac{1}{2}[\varepsilon_p + \varepsilon_d - \sqrt{(\varepsilon_p - \varepsilon_d)^2 + 16t_{pd}^2 r_0^2 \gamma_k^2}], \quad (7)$$

$$E_2(k) = \frac{1}{2}[\varepsilon_p + \varepsilon_d + \sqrt{(\varepsilon_p - \varepsilon_d)^2 + 16t_{pd}^2 r_0^2 \gamma_k^2}], \quad (8)$$

$$E_3(k) = \varepsilon_p, \quad (9)$$

where  $\gamma_k^2 \equiv \sin^2(k_x/2) + \sin^2(k_y/2)$ . In this simplified situation the matrices  $U$  assume the form reported in Eq. (8) of the companion paper and the self-consistency equations can be written in a more explicit way:

$$\lambda_0 = \frac{1}{N_s} \sum_k \frac{4t_{pd}^2 \gamma_k^2}{R_k} (f_{1k} - f_{2k}), \quad (10)$$

$$q_0 = r_0^2 + \frac{1}{N_s} \sum_k (u_k^2 f_{1k} + v_k^2 f_{2k}), \quad (11)$$

$$X_0 - Y_0 = -2Vn_d = -\frac{2V}{N_s} \sum_k (u_k^2 f_{1k} + v_k^2 f_{2k}), \quad (12)$$

$$X_0 + Y_0 = 2Vn_p = \frac{2V}{N_s} \sum_k (v_k^2 f_{1k} + u_k^2 f_{2k} + f_{3k}), \quad (13)$$

$$q_0(1+\delta) = \frac{1}{N_s} \sum_k (f_{1k} + f_{2k} + f_{3k}), \quad (14)$$

where  $u_k^2 \equiv \frac{1}{2}[1 + (\varepsilon_p - \varepsilon_d)/R_k]$ ,  $v_k^2 \equiv \frac{1}{2}[1 - (\varepsilon_p - \varepsilon_d)/R_k]$  with  $R_k^2 \equiv (\varepsilon_p - \varepsilon_d)^2 + 16t_{pd}^2 r_0^2 \gamma_k^2$ , and  $f_{lk} \equiv f[E_l(k) - \mu]$  [compare expressions after Eq. (3) of the companion paper].

The analogy at the mean-field level between the extended Hubbard model and the Ising model discussed in the weak-coupling framework<sup>4</sup> can be extended to the present strong-coupling context, the main difference is the presence of the constraint, which now forbids copper occupancies larger than  $q_0 N$ , forcing  $r_0^2$  to be a non-negative quantity.

The Curie-Weiss-like equation can more conveniently be expressed in terms of  $r_0^2$  rather than in terms of the ‘‘magnetization’’  $n_p - n_d$ . This latter quantity can be rewritten by exploiting the constraint and the total particle number condition Eqs. (11) and (14):

$$n_p - n_d = -q_0 \left[ 1 - \delta - 2 \frac{r_0^2}{q_0} \right].$$

Then, defining the Hartree gap

$$\Delta_H \equiv \varepsilon_p^0 - \varepsilon_d^0 + 2V(n_d - n_p),$$

the above expression represents a straight line in the  $\Delta_H - r_0^2$  plane,

$$r_0^2 = -\frac{1}{4V} \Delta_H + \frac{1}{4V} [\Delta_0 + 2Vq_0(1-\delta)] \quad (15)$$

with  $\Delta_0 \equiv \varepsilon_p^0 - \varepsilon_d^0$ .

The self-consistency problem is then solved by finding the intersection(s) of the straight line Eq. (15) with the curve  $r_0^2 = r_0^2(\Delta_H, \delta)$  obtained by solving Eqs. (10) and (11) together with condition (14) for all the values of  $\Delta_H$ . We show  $r_0^2(\Delta_H)$  in Fig. 1 at doping  $\delta = 0$  and 0.2 together with the straight line at zero doping.

It should be recognized that the curve  $r_0^2 = r_0^2(\Delta_H, \delta)$  no longer depends on  $V$ : the same curve would be obtained in the three-band Hubbard model (without  $V$ ) (Ref. 8) by simply varying the bare CT gap  $\Delta_0$ . On the other hand, the angular coefficient of the straight line (15) is  $1/(4V)$  so that the number of intersections depends on  $V$ . Then a critical value  $V^*(\delta)$  exists such that, for  $V < V^*(\delta)$ , the straight line is too steep and only intersects once the curve  $r_0^2 = r_0^2(\Delta_H, \delta)$ . If  $V > V^*(\delta)$ , instead, three solutions occur corresponding to one maximum and two minima in the free-energy functional. In

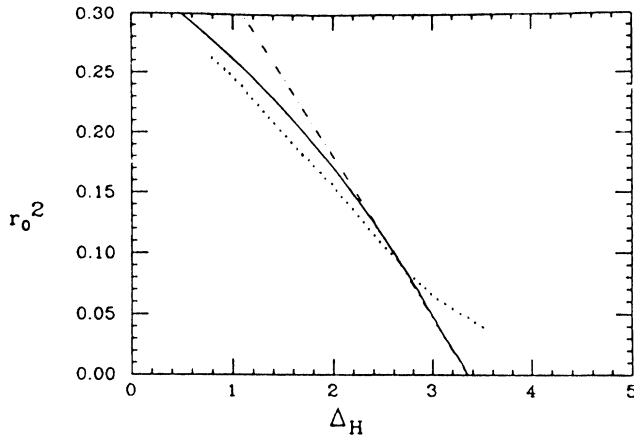


FIG. 1.  $r_0^2$  vs  $\Delta_H$  for doping  $\delta=0$  and  $0.2$ . The straight line is given by Eq. (15) in the text defining the critical slope at which the mean-field equations cease to have a unique solution. All energies are in units of  $t_{pd}$  (from Ref. 2).

particular, in the case with  $t_{pp}=0$ ,  $\delta=0$ ,  $V^* \approx 1.76t_{pd}$ .

When  $V > V^*(\delta)$ , with increasing doping, the mean-field solution presents a first-order valence transition from a  $d$ -like metal minimum with a small  $r_0^2$  to a  $p$ -like metal minimum with a larger  $r_0^2$ .

The MCTI transition is affected by the presence of the valence transition: while the MCTI transition is second order when  $V < V^*$ , it becomes first order when  $V > V^*$ .<sup>9</sup> In this latter case the valence transition line in the plane  $\Delta_0 - \delta$  starts from the MCTI transition point.

Notice that the mean-field equations (10)–(14) describe the system at fixed doping, in the absence of homogeneous density fluctuations. Then the fact that the mean-field equations exhibit a valence change varying the doping is indicative that allowing density fluctuations can result in phase separation between  $d$ -like and  $p$ -like phases. This occurrence can easily be investigated in the grand canonical ensemble by studying the density-density correlation functions at a fixed chemical potential. This analysis requires the calculation of the Gaussian fluctuations ( $1/N$  corrections) of the boson fields. In fact, the boson propagators enter the diagrammatic structure of both the total density and the CT density correlation functions at leading order. This calculation will be described in the next section.

The presence of a phase separation in the system can also be revealed by a mean-field calculation of the chemical potential as a function of doping. A typical case is shown in Fig. 2, where it is apparent that the chemical potential is not a monotonically increasing function of the number of particles. In particular, there are points where the inverse compressibility  $\chi^{-1} \equiv d\mu/dn$  is zero. A diverging compressibility is a signature of phase separation requiring the use of a standard Maxwell construction to determine the stable region in the phase diagram.

It is important to realize that, when the compressibility diverges (that is, the static total density fluctuations diverge), the static CT susceptibility  $\chi_{CT}$  also diverges because the total density and the CT modes are coupled.<sup>1</sup>

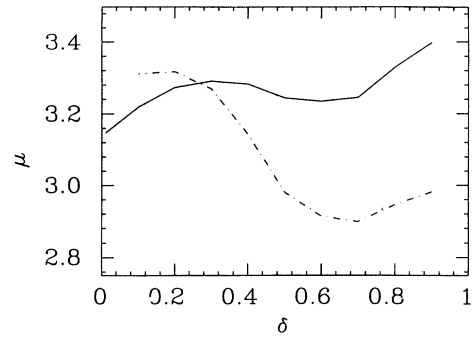


FIG. 2. Chemical potential as a function of doping for  $t_{pp}=0.2t_{pd}$ ,  $\Delta_0=2.3t_{pd}$ , and  $V=2.3t_{pd}$  for  $U_p=2t_{pd}$  (solid line) and  $U_p=0$  (dash-dotted line).

This is intuitively seen by noting that a decoupled CT mode means that the intracell charge fluctuates from copper to the surrounding oxygens and vice versa with  $\delta n_{d_i} + \delta n_{p_i} = 0$ . On the other hand, the Hubbard repulsion depresses the charge fluctuations on copper, which have to satisfy a constraint. This strongly favors a CT mode accompanied by a total intracell charge fluctuation  $\delta n_{d_i} + \delta n_{p_i} \neq 0$  because copper cannot always accept all of the charge that oxygen “would like” to give to it. A deeper insight into the interplay between the CT and the density modes requires the dynamical analysis which has been presented in the companion paper in the weak-coupling limit and which will be reconsidered in the following sections in the strong-coupling limit.

Mean-field phase diagrams for two typical sets of parameters are shown in Fig. 3, where the dashed lines indicate the points where the compressibility and the CT susceptibility become infinite. Figure 3 (from Refs. 1 and 2) is for  $V < V^*$  and shows that phase separation can occur even in the absence of a valence transition. In the simple case  $t_{pp}=0$  the minimum value for  $V$  at which phase separation occurs is

$$V_{\min} = (2/\sqrt{\gamma_2})(\gamma_4/\gamma_2 - 1)^{1/2}t_{pd} \approx 1.63t_{pd}.$$

$\gamma_2 \equiv (1/N_s) \sum_k \gamma_k^2$  and  $\gamma_4 \equiv (1/N_s) \sum_k \gamma_k^4$ , the sum being

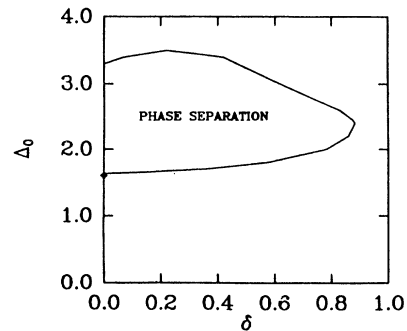


FIG. 3. Phase diagram  $\Delta_0/t_{pd}$  vs  $\delta$  for  $t_{pp}=0$ ,  $U_p=0$ , and  $V=1.75t_{pd}$ . The diamond indicates the metal CT insulator transition point (from Ref. 1).

extended to the occupied  $k$  states at  $\delta=0$ . These expression will be derived in Sec. IV.

On the other hand, Figs. 4–6, where  $V > V^*$ , show the presence of a first-order transition line ending with a critical point (indicated by a dot). By increasing  $V > V^*$  this transition line becomes longer and the critical point moves away from the MCTI transition point deeper and deeper inside the unstable region. Even though the critical point lays inside the physically inaccessible region of negative compressibility, it is nevertheless instructive to notice that this point is in some sense reminiscent of the MCTI transition point at  $V < V^*$ . In fact, not only the critical point continuously evolved from the MCTI point when  $V$  exceeds  $V^*$ , but also at both the MCTI point when  $V < V^*$  and at the critical point when  $V > V^*$  the compressibility goes to zero. In both cases the excitonic mode becomes soft and the zero momentum dynamical scattering amplitude  $\Gamma_\omega$  diverges as we shall see in the next section. Notice, however, that away from half filling  $r_0$  is not critical.

In the phase diagram of Fig. 4 both  $t_{pp}$  and  $U_p$  are different from zero. We find that  $t_{pp}$  stabilizes the region at small doping, while  $U_p$  stabilizes the region at high doping. By varying  $t_{pp}$  and  $U_p$  we can tune to a large extent the values of the doping involved in the phase-separation region. For the purpose of calculating these phase diagrams the oxygen oxygen repulsion  $U_p$  was introduced. The model with finite  $U_p$  is still soluble in the large- $N$  limit and the large- $N$  solution is equivalent to treating  $U_p$  at the level of the Hartree approximation.

Similar results are obtained at negative doping for which a phase diagram is reported in Fig. 5. Comparing this latter phase diagram with the one in Fig. 3 it is apparent that the instability region extends on a much smaller region.

The strong-coupling formalism described at the beginning of this subsection does not allow for exchange effects at lowest order in perturbation theory. It is, in fact, apparent that the mean-field treatment of the Hubbard-Stratonovich decoupling is equivalent to the Hartree decoupling only, without any Fock term. In order to

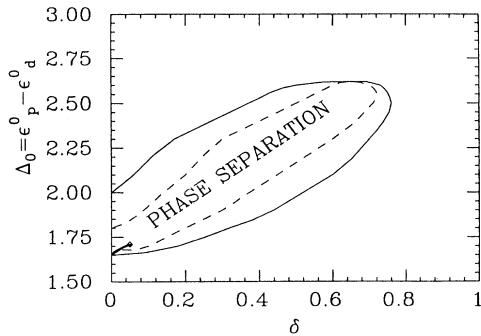


FIG. 4. Phase diagram  $\Delta_0/t_{pd}$  vs  $\delta$  for  $t_{pp}=0.2t_{pd}$ ,  $U_p=2.0t_{pd}$ , and  $V=2.3t_{pd}$ . The first-order  $p$ - $d$  valence transition is shown by a thick line ending with a critical point indicated by the diamond. The metal CT insulator transition is first order and occurs at the crossing point between the vertical axis and valence transition line.

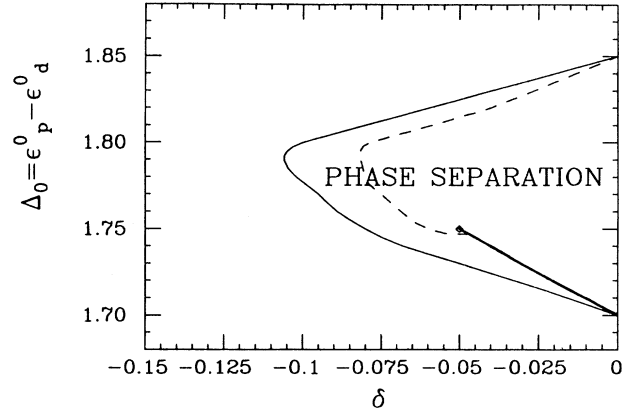


FIG. 5. Phase diagram  $\Delta_0/t_{pd}$  vs  $\delta$  for  $t_{pp}=0.2t_{pd}$ ,  $U_p=0$ , and  $V=2.3t_{pd}$  in the case of negative (electron) doping. The first-order  $p$ - $d$  valence transition and the metal CT insulator transition are shown as in Fig. 4.

consider these effects already at the mean-field level, we have included “by hand” in the Hamiltonian a term of the type

$$H_{V_2} = \frac{V_2}{N} \sum_{i,\sigma,\sigma'} d_{i\sigma}^\dagger d_{i\sigma'} p_{i\eta\sigma'}^\dagger p_{i\eta\sigma} \cdot$$

$\eta = \pm x, \pm y$

This additional term can be decoupled by means of a complex Hubbard-Stratonovich field  $Z_{i\eta}$ , for which one can choose a mean-field solution of the form

$$\langle Z_{i\eta} \rangle = \frac{V_2}{N} \sum_{\sigma} \text{sgn}(\eta) \langle p_{i\eta\sigma} d_{i\sigma}^\dagger \rangle = V_2 \text{sgn}(\eta) \left[ \frac{r_0 \lambda_0}{4t_{pd}} \right]$$

defined on the bond between site  $i$  and site  $i+\eta$ .<sup>10</sup> This term additively modifies the hopping resulting in an additional Fock renormalization of the mean-field band structure. This also results in a modification of the value for  $V^*$ , giving, when  $t_{pp}=0$ ,

$$V^* = \frac{\gamma_4}{(\gamma_2)(3/2)} t_{pd} + \frac{\gamma_4}{2\gamma_2} V_2$$

$$= 1.76t_{pd} + 0.73V_2 = 2.762t_{pd} \cdot$$

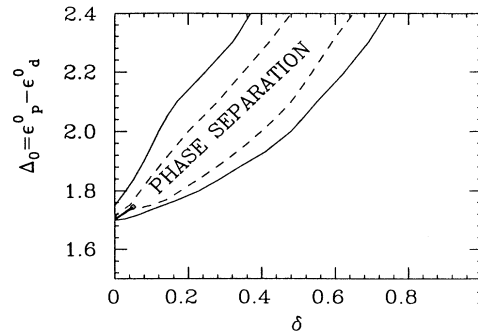


FIG. 6. Phase diagram  $\Delta_0/t_{pd}$  vs  $\delta$  for  $t_{pp}=0.2t_{pd}$ ,  $U_p=2t_{pd}$ ,  $V=3t_{pd}$ , and  $V_2=1.1t_{pd}$ . The first-order  $p$ - $d$  valence transition and the metal CT insulator transition are shown as in Fig. 4.

The phase diagram for the case  $V=3t_{pd}$ ,  $U_p=2t_{pd}$ ,  $t_{pp}=0.2t_{pd}$ , and  $V_2=1.1t_{pd}$  is reported in Fig. 6. By comparing this phase diagram with Fig. 3 we infer that the Fock contributions introduced via  $V_2$  have an effect similar to that of  $t_{pp}\neq 0$  and stabilize the system at small doping. We have found that for generic values of the parameters (that is, not too close to the metal-charge-transfer-insulator transition),  $V_2$  does not modify qualitatively the mean-field picture discussed above, but introduces some quantitative modifications. The effects of this term near the transition have been recently examined by Hicks, Ruckenstein, and Schmitt-Rink using an equation of motion method. They have shown that for  $V=V^*=2V_2$ ,  $U_p=t_{pp}=0$ , the lower and the upper curves of infinite compressibility join at small but nonzero doping. For these values of the parameters the strong-coupling phase diagram is more like the weak-coupling phase diagram.

The presence of long-range Coulombic forces would, of course, prevent the formation of macroscopically large phase-separated regions with different concentrations of holes. In the real systems, however, the negatively charged oxygen ions are rather mobile, so that the hole phase separation could occur if the  $O^{-2}$  ions can also separate compensating for the charge imbalance. In this context the particular shape of the unstable region in Figs. 4 and 6 is particularly appealing since it indicates the possibility of having a stable region in the higher part of the diagram at low and intermediate doping followed by a phase-separation region at larger doping. A similar behavior has been reported in  $La_{2-x}Sr_xCuO_4$ ,<sup>11</sup> where the phase separation occurs between a low-doping metallic phase, which becomes superconducting, and a metallic nonsuperconducting phase at high doping. The phase diagram of Fig. 4 could provide an explanation of electronic origin if the phase separation in the strontium-doped lanthanum copper oxide is confirmed.

Notice that relevant role in the phase diagrams described above is played by the MCTI transition, close to which the kinetic energy is so strongly depressed that it is no longer able to stabilize the system. A similar situation is present in the three-band extended Hubbard model with  $V=0$  in the presence of a Heisenberg magnetic coupling (two-band  $t$ - $J$  model).<sup>12</sup> In this latter model the existence of a phase separation of a different origin than the one discussed in the present context has been shown in analogy with the single-band  $t$ - $J$  model.<sup>13</sup> In particular, the kinetic-energy suppression due to the MCTI transition resulted in a low-doping region where the system separated into a metallic paramagnetic phase and an anti-ferromagnetic insulating half-filled phase. This occurrence could, then, account for the phase separation observed in overoxygenated  $La_2CuO_{4+\delta}$  compounds. In principle, a third scenario, in which both phase separations, the one at low doping of magnetic origin and the one at larger doping of excitonic origin, can occur in the same compound. No experimental evidence is, however, available to support this lattice hypothesis.

We conclude this subsection commenting on the limitations of our large- $N$  analysis due to the fact that magnetism is not included, at least at the level of mean-field and

$1/N$  corrections. The absence of magnetism makes our mean-field picture rather incomplete and unrealistic at low doping. However, it is possible to estimate the doping above which the effects of the magnetic interactions cease to be relevant. In particular, we performed the following analysis. In the absence of  $V$  we introduced a magnetic term in the Hamiltonian of the type

$$H_J = \frac{J}{N} \sum_{ij\sigma\sigma'} d_{i\sigma}^\dagger d_{j\sigma} d_{j\sigma'}^\dagger d_{i\sigma'}$$

and we introduced the standard mean-field decoupling  $\Delta_{ij} = (J/N) \sum_{\sigma} \langle d_{i\sigma}^\dagger d_{j\sigma} \rangle$ . Then we identified for various values of the parameters  $t_{pd}$  and  $\epsilon_p^0 - \epsilon_d^0$  the doping at which the uniform mean-field solution ( $\Delta_{ii\pm x} = \Delta_{ii\pm y} = \Delta$ ) is energetically more favorable than other simple magnetic solutions (e.g., the dimer solutions  $\Delta_{ii+x} = \Delta_1$ ,  $\Delta_{ii\pm y} = \Delta_2$ , and  $\Delta_{ii-x} = \Delta_3$ ), which mimic long-range-ordered magnetic phases. Above this doping the system is a Fermi liquid in the presence of magnetic correlations described by a mean-field parameter  $\Delta$ . The effect of magnetic correlations can be thought to be unessential (at least to the charge degrees of freedom) when corrections to the band structure due to  $\Delta$  do not sizably modify the band structure obtained in the absence of  $H_J$ . Typically we find that, for a value of  $J$  corresponding to a physical Heisenberg coupling of about 0.1 eV, the magnetic effects seem to be irrelevant (at least as far as the mean-field band structure is concerned) at a doping  $\delta \approx 0.15$  or even less. Specifically, for typical values of the parameters ( $V=0$ ,  $\Delta_0=5t_{pd}$ ) we obtain for the bandwidth ratio  $W(J=0.1t_{pd})/W(J=0) \approx 1.29$  at  $\delta=0.14$  and  $W(J=0.1t_{pd})/W(J=0) \approx 1.18$  at  $\delta=0.2$ , showing that already at doping as low as  $\delta=0.14$  less than 30% of the bandwidth is due to the presence of  $J$ .

We believe, therefore, that magnetic effects can be safely neglected in analyzing the extended Hubbard model and its CTI down to doping as low as 0.15.<sup>14</sup>

Moreover, the main physical insight which can be gained from the large- $N$  analysis on the charge degrees of freedom and on their high-energy behavior will hold to a large extent irrespectively of the presence of magnetism and therefore of the value of  $\delta$ .

## B. Dynamics

The mean-field analysis of the strong-coupling ( $U_d = \infty$ ) limit shows that a sizable  $V$  leads to a divergence of both CT susceptibility and compressibility. In Ref. 1, Grilli *et al.* also evaluated the effective Cooper coupling constant, which is mediated by the Gaussian fluctuations of the mean-field variables, and found  $s$ -wave and  $d$ -wave pairing close but outside the phase-separation region. Since the calculation of the coupling constant was done in the static limit, the dynamical origin of the pairing was not elucidated. It is important to understand the frequency dependence of the coupling in view of an Eliashberg type of analysis. In the weak-coupling case, the low-energy CT excitonic mode is found effective in inducing the superconducting pairing near CTI.<sup>15-17</sup> But, as  $U_d$  increases, this CT excitonic mode is pushed away

to high energy. Nevertheless, in the strong-coupling limit, where  $U_d$  is set to infinity, phase separation and superconducting pairing are still found to exist. In order to clarify this apparent contradiction and to fully understand the dynamics of the instabilities and of the pairing, we need to calculate the frequency dependence of the density-density correlation functions and of the effective interaction in the Cooper channel. We note that the  $X$  and  $Y$  fields introduced to decompose  $Vn_p n_d$  and the  $\lambda$  and  $b$  fields implementing the constraint allow only  $A_{1g}$  and  $B_{1g}$  symmetry fluctuations. However, this is enough to see the dynamics of zero sound and the CT exciton in analogy with our simplified formalism in the weak-coupling limit.

In the strong-coupling framework, we evaluate the collective modes and the dynamical susceptibilities at leading order in the  $1/N$  expansion. This requires summing ring diagrams with fermionic bubbles (of order  $N$  due to the spin summation) directly connected by boson propagators (order  $1/N$ ). The various susceptibilities, when defined per unit spin, will then be exact to order  $(1/N)^0$ .

It must be noted that, within the present  $1/N$  expansion, no self-energy insertion of boson propagators into the fermionic Green functions and no bubble exchange diagrams are allowed at this order. For this reason the only instability that we have detected in the model is the CTI one: the spin-density-wave and the charge-density-wave instabilities that show up in the random-phase approximation of the weak-coupling approach cannot occur in the present context. In fact, spin-density waves can only result from an effective magnetic coupling which is generated in the  $1/N$  expansion by a double exchange of bosons at order  $(1/N)^2$ . The charge-density wave, instead, is an instability occurring at  $\mathbf{Q}=(\pi, \pi)$  and is suppressed in the absence of exchange diagrams because  $V(\mathbf{q}=\mathbf{Q})=0$  in the direct diagrams. In the following we take  $V_2=0$  for the sake of simplicity.<sup>18</sup> We start our

analysis by deriving the  $1/N$  Gaussian expression of the boson propagators.

In order to write the Hamiltonian of our system of coupled fermion and boson fields  $H=H_{\text{MF}}+H_{\text{bos}}+H_{\text{int}}$  in a compact form we define a four-component field  $A^\mu=(\delta r, \delta \lambda, \delta X, \delta Y)$  formed by the part of the boson fields fluctuating around the saddle-point solution

$$r_i = r_0(1 + \delta r_i),$$

$$\lambda_i = -i\lambda_0 + \delta \lambda_i,$$

$$X_i = X_0 + \delta X_i,$$

$$Y_i = -iY_0 + \delta Y_i.$$

The field  $A^\mu$  is a function of both space and time  $A^\mu = A_i^\mu(\tau)$ . As usual, in the zero-temperature limit the Matsubara time  $-i\tau$  and the Matsubara frequencies  $i\omega_m = i2m\pi T$  have to be substituted by the real time and the real frequencies.

In terms of the Fourier-transformed field  $A^\mu(q)$  the purely bosonic part of the Hamiltonian assumes the form

$$H_{\text{bos}} = N \sum_{q\mu\nu} A^\mu(q) B^{\mu\nu}(q) A^\nu(-q).$$

To simplify the notation here and in the following the time dependence is not explicitly written. A simple inspection of Eq. (5) shows that the matrix  $B^{\mu\nu}$  has all elements equal to zero except for  $B^{1,1} = r_0^2 \lambda_0$ ,  $B^{1,2} = B^{2,1} = ir_0^2$ ,  $B^{3,3} = B^{4,4} = 1/2V$ .

We then use the basis set  $\Psi_{k\sigma\alpha} \equiv (d_{k\sigma}, ip_{xk\sigma}, ip_{yk\sigma})$  of three-component fermionic fields. In this basis the mean-field (order  $N$ ) fermionic Hamiltonian has matrix elements

$$H_{\text{MF}}(k) = \begin{pmatrix} \varepsilon_d & -2r_0 t_{pd} \sin(k_x/2) & -2r_0 t_{pd} \sin(k_y/2) \\ -2r_0 t_{pd} \sin(k_x/2) & \varepsilon_p & -2t_{pp} \beta_k \\ -2r_0 t_{pd} \sin(k_y/2) & -2t_{pp} \beta_k & \varepsilon_p \end{pmatrix},$$

where  $\beta_k \equiv 2 \sin(k_x/2) \sin(k_y/2)$ . This matrix can be diagonalized in order to obtain the bands reported in Sec. II A. The diagonalizing unitary transformation  $U(k)$  allows one to then transform to the quasiparticle basis  $\tilde{\Psi}_{k\sigma\alpha} = \sum_{\beta} U_{\alpha\beta}(k) \Psi_{k\sigma\beta}$  so that

$$H_{\text{MF}} = \sum_{k\sigma\alpha\beta} H_{\text{MF}}^{\alpha\beta}(k) \Psi_{k\sigma\alpha}^\dagger \Psi_{k\sigma\beta} = \sum_{k\sigma\alpha} E_\alpha(k) \tilde{\Psi}_{k\sigma\alpha}^\dagger \tilde{\Psi}_{k\sigma\alpha}.$$

The boson-fermion interaction term can then be cast in the form

$$H_{\text{int}} = \sum_{k,q,\sigma} \Psi_{k+(q/2)\sigma}^\dagger \Lambda^\mu(k,q) \Psi_{k-(q/2)\sigma} A^\mu(q) = \sum_{k,q,\sigma} \tilde{\Psi}_{k+(q/2)\sigma}^\dagger \tilde{\Lambda}^\mu(k,q) \tilde{\Psi}_{k-(q/2)\sigma} A^\mu(q),$$

where the fermion component index has been dropped and the  $(3 \times 3)$  boson-fermion interaction vertices  $\Lambda^\mu$  in the orbital operator basis can be obtained from Eq. (5):

$$\Lambda^1 = -2r_0 t_{pd} \begin{pmatrix} 0 & \sin\left[\frac{k_x - q_x/2}{2}\right] & \sin\left[\frac{k_y - q_y/2}{2}\right] \\ \sin\left[\frac{k_x + q_x/2}{2}\right] & 0 & 0 \\ \sin\left[\frac{k_y + q_y/2}{2}\right] & 0 & 0 \end{pmatrix}, \quad \Lambda^2 = \begin{pmatrix} i & 0 & 0 \\ 0 & 0 & 0 \\ 0 & 0 & 0 \end{pmatrix},$$

$$\Lambda^3 = \begin{pmatrix} 1 & 0 & 0 \\ 0 & -\cos\frac{qx}{2} & 0 \\ 0 & 0 & -\cos\frac{qy}{2} \end{pmatrix}, \quad \Lambda^4 = \begin{pmatrix} i & 0 & 0 \\ 0 & i\cos\frac{qx}{2} & 0 \\ 0 & 0 & i\cos\frac{qy}{2} \end{pmatrix},$$
(16)

while the quasiparticle vertices  $\tilde{\Lambda}_{\alpha\beta}^\mu(k, q)$  are defined as

$$\tilde{\Lambda}^\mu(k, q) = U \left[ k + \frac{q}{2} \right] \Lambda^\mu(k, q) U^\dagger \left[ k - \frac{q}{2} \right]. \quad (17)$$

The propagators of the  $A$  field are given by

$$D^{\mu\nu}(q, \omega_m) = \langle A^\mu(q, \omega_m) A^\nu(-q, -\omega_m) \rangle \\ = N^{-1} [2B + \Pi(q, \omega_m)]_{\mu\nu}^{-1} \quad (18)$$

with

$$\Pi^{\mu\nu}(q, \omega_m) = \sum_{k, \alpha, \beta} \frac{f[E_\alpha(k + q/2)] - f[E_\beta(k - q/2)]}{E_\alpha(k + q/2) - E_\beta(k - q/2) - i\omega_m} \\ \times \tilde{\Lambda}_{\alpha\beta}^\mu(k, q) \tilde{\Lambda}_{\beta\alpha}^\nu(k, -q). \quad (19)$$

The factor 2 appearing in the denominator of  $D^{\mu\nu}(q, \omega_m)$  is due to the fact that the bosonic fields in the presently used radial gauge are real.

Within the present formalism it is also possible to define the effective scattering amplitude between the quasiparticles in the lowest band

$$\Gamma(k, k'; q, \omega) = -\tilde{\Lambda}_{11}^\mu(k', -q) D^{\mu\nu}(q, \omega) \tilde{\Lambda}_{11}^\nu(k, q). \quad (20)$$

Then the scattering amplitude in the Cooper channel can be specified as

$$\Gamma(k, k'; \omega) \\ = - \sum_{\mu\nu} \tilde{\Lambda}^\mu(k, k') D^{\mu\nu}(q = k - k', \omega) \tilde{\Lambda}^\nu(-k, -k'). \quad (21)$$

Notice that, the boson propagator being of order  $1/N$ , the scattering amplitudes are of the same order. On the other hand, since the bare polarization bubbles are of order  $N$ , the matrix form of the density-density correlation function at leading order is given by

$$P_{\alpha\beta}(q, \omega) = \frac{1}{N} \sum_{\sigma\sigma'} \langle n_{\alpha\sigma}(q) n_{\beta\sigma'}(-q) \rangle \\ = P_{\alpha\beta}^0(q, \omega) \\ + N \sum_{\mu\nu} \chi_{\alpha\mu}^0(q, \omega) D^{\mu\nu}(q, \omega) \chi_{\nu\beta}^0(q, \omega), \quad (22)$$

where

$$P_{\alpha\beta}^0(q, \omega) = \frac{1}{N} \sum_{\sigma\sigma'} \langle n_{\alpha\sigma}(q) n_{\beta\sigma'}(-q) \rangle_0 \quad (23)$$

is the bare density-density correlation functions, and

$$\chi_{\alpha\mu}^0(q, \omega) \\ = \frac{1}{N} \sum_{\sigma\sigma'} \left\langle n_{\alpha\sigma}(q) \sum_{k; \gamma, \delta} \Psi_{k\sigma'\gamma}^\dagger \Lambda_{\gamma\delta}^\mu(k, q) \Psi_{k+q\sigma'\delta} \right\rangle_0, \quad (24)$$

where  $\alpha = d, p_x, p_y$ , and  $\mu = 1, 2, 3$ , and 4. Linearly combining  $P_{\alpha\beta}(q, \omega)$ , one can calculate the total density-density correlation function  $\chi(q, \omega) \equiv \langle (n_p + n_d)(n_p + n_d) \rangle$  and the charge-transfer susceptibility  $\chi_{CT} \equiv \langle (n_p - n_d)(n_p - n_d) \rangle$ .

### III. THE COLLECTIVE MODES

The above definitions complete the set of formal tools needed to calculate diagrammatically the various correlation functions. In particular, the CT and the total density dynamical susceptibilities per unit spin  $\chi_{CT}(q, \omega)$  and  $\chi(q, \omega)$  can be obtained from Eqs. (22)–(24). More simply they can be extracted from the  $XX$  and  $YY$  propagators according to the following relations:

$$D^{33}(q, \omega) = \frac{1}{N} [V + V^2 \chi_{CT}(q, \omega)], \quad (25)$$

$$D^{44}(q, \omega) = \frac{q}{N} [V - V^2 \chi(q, \omega)]. \quad (26)$$

Notice also that the poles of the  $\chi$ 's, describing (possible) collective modes, coincide with the poles of  $D^{\mu\nu}(q, \omega)$ .  $D^{\mu\nu}(q, \omega)$  therefore contains all the relevant information we need. Specifically all the possible resonances out of the continuum are the zeroes  $\omega = \omega(q)$  of  $\det D^{-1}(q, \omega)$ , i.e., their dispersions satisfy the equation

$$\det(2B + \Pi) = 0. \quad (27)$$

From a dynamical point of view the CT physics is characterized by the presence of a fluctuating nonconserved field,  $n_d - n_p$ , coupled to a fluctuating conserved field,  $n_d + n_p$ . The density fluctuations give rise, if propagating, to the zero-sound mode, i.e., to a massless mode.

On the other hand, the  $p$ - $d$  CT fluctuations, being described by a nonconserved field, will contribute to the exciton "optical-like" mode.

The energy  $\omega_{\text{exc}}$  of the excitonic mode in the small- $q$  limit can be evaluated by putting  $q=0$  in Eq. (27). This strongly simplifies the analytical computation. In fact, setting  $q=0$  (while leaving  $\omega$  finite) eliminates all the intraband contributions to  $D^{\mu\nu}(0,\omega)$ . This reflects the peculiarity of the  $q=0$  limit which decouples

$$\begin{aligned} \rho(q) &= n_d(q) + n_p(q) \\ &= (1/\sqrt{N_s}) \sum_k \tilde{\Psi}_{k+(q/2)\sigma}^\dagger \tilde{\Lambda}^4(k,q) \tilde{\Psi}_{k-(q/2)\sigma} \end{aligned}$$

from the dynamics because of particle conservation. All contributions to  $D^{\mu\nu}(0,\omega)$  therefore come from interband transitions. Thus the only vertices that are needed in the evaluation of  $\Pi^{\mu\nu}(0,\omega)$  are  $\tilde{\Lambda}_{12}^\mu(q=0)$  and  $\tilde{\Lambda}_{13}^\mu(q=0)$ . In the following we shall assume a vanishing oxygen-oxygen overlap,  $t_{pp}=0$ . In this case the evaluation of the determinant in Eq. (27) is further simplified by the specific form of the vertices  $\tilde{\Lambda}^\mu(q=0)$ : all vertices depend on  $k$  via  $\gamma_k$  and have the same  $k$  dependence apart from constant factors. Moreover, a simple inspection shows that the  $\tilde{\Lambda}_{13}^\mu(q=0)$  vertices vanish identically while

$$\tilde{\Lambda}_{12}^\mu(k,q=0) = \frac{2r_0 t_{pd} \gamma_k}{R_k} \begin{pmatrix} \Delta \\ i \\ 2 \\ 0 \end{pmatrix}.$$

$$D^{-1}(q=0,\omega) = 2Nr_0^2 \begin{pmatrix} \lambda_0 - \Delta^2 I & i(1 - \Delta I) & -2\Delta I & 0 \\ i(1 - \Delta I) & I & -2iI & 0 \\ -2\Delta I & -2iI & 1/(2r_0^2 V) - 4I & 0 \\ 0 & 0 & 0 & 1/(2r_0^2 V) \end{pmatrix}$$

and the determinant can be evaluated as

$$\begin{aligned} \det \frac{1}{N} D^{-1}(0,\omega) &= \left[ \frac{2r_0^2}{V} \right]^2 [1 - (2\Delta - \lambda_0 + 8r_0^2 V) I(\omega)]. \quad (28) \end{aligned}$$

Equation (28) allows for a single resonant mode describing a resonant emission and absorption of interband particle-hole pairs (the CT mode). The mode will be a bound state or an antibound one with respect to the interband quasiparticle gap depending on  $(2\Delta - \lambda_0 + 8r_0^2 V)$  being positive or negative, respectively.<sup>19</sup>

To proceed further analytically it is necessary to resort to some approximation and therefore we will assume to be at low doping deep inside the region of parameters that give an insulating system at half filling. In this region one can take  $r_0$  to be small. To make easily readable the small- $r_0$  limit,  $I(\omega)$  can conveniently be rewritten as

$$I(\omega) = \frac{\lambda_0}{\Delta^2 - \omega^2} [1 - \alpha(\omega)r_0^2] \quad (29)$$

These facts allow one to express  $\Pi^{\mu\nu}$  in terms of a single interband integral  $I(\omega)$ :

$$\Pi^{\mu\nu}(q=0,\omega) = -2r_0^2 \begin{pmatrix} \Delta^2 & i\Delta & 2\Delta & 0 \\ i\Delta & -1 & 2i & 0 \\ 2\Delta & 2i & 4 & 0 \\ 0 & 0 & 0 & 0 \end{pmatrix} I(\omega),$$

where

$$I(\omega) = \frac{1}{N_s} \sum_k \frac{4t_{pd}^2 \gamma_k^2}{R_k (R_k^2 - \omega^2)}.$$

The proportionality between the various bubbles leads to the remarkable property that  $I(\omega)$  appears at most linearly in  $\det D^{-1}$ , while all contributions that are of higher order in  $I(\omega)$  cancel. This is because the matrix  $\Pi^{\mu\nu}$  has a range one in the particular limit  $q=0$  reflecting the invariances of the fermion problem in the external fields  $r$ ,  $\lambda$ ,  $X$ , and  $Y$ . At  $q=0$ , both the total density  $\rho$  and the fermion energy  $H_{\text{MF}}$  are conserved quantities.  $r$  and  $\lambda$  being coupled to the hopping term and to the  $d$  density, respectively, it is direct to show that the boson fields are only coupled to  $n_d - n_p$  in the combination  $\frac{1}{2}(i\lambda + \Delta r) + X$ , while  $8r_0^2 I(\omega)$  is the single bubble contribution  $\chi_{\text{CT}}^0(0,\omega)$  to  $\chi_{\text{CT}}(0,\omega)$ . We note that the absence in  $\det D^{-1}$  of terms higher order in  $I(\omega)$  will result in the presence of only one optical mode.

The final expression for  $D^{-1}$  can be obtained from Eq. (18):

with

$$\alpha(\omega) \equiv \frac{1}{\lambda_0 N_s} \sum_k \frac{64t_{pd}^4 \gamma_k^4}{R_k (R_k^2 - \omega^2)}$$

so that the determinant assumes the form

$$\begin{aligned} \det \frac{1}{N} D^{-1}(0,\omega) &= \left[ \frac{2r_0^2}{V} \right]^2 \frac{1}{\Delta^2 - \omega^2} \\ &\times \{ (\Delta - \lambda_0)^2 - \omega^2 \\ &+ r_0^2 \lambda_0 [\alpha(\omega)(2\Delta - \lambda_0) - 8V] \}. \quad (30) \end{aligned}$$

By expanding  $\alpha(\omega)$  in powers of  $r_0$ , one gets

$$\alpha(\omega) \approx \frac{16t_{pd}^2 \gamma_4}{\gamma_2} \frac{1}{\Delta^2 - \omega^2} \quad (31)$$

with  $\gamma_2 \equiv (1/N_s) \sum_k \gamma_k^2 = \frac{1}{2} + 2/\pi^2$  and  $\gamma_4 \equiv (1/N_s) \sum_k \gamma_k^4 = \frac{5}{8} + 4/\pi^2$ . Using Eq. (31) one can solve Eq. (27) to order  $r_0^2$ :

$$\omega_{\text{exc}}^2 \approx (\Delta - \lambda_0)^2 + r_0^2 \lambda_0 [\alpha(\omega = |\Delta - \lambda_0|)(2\Delta - \lambda_0) - 8V]. \quad (32)$$

Equation (32) shows that near the insulating regime,  $r_0^2 = 0$ ,  $\omega_{\text{exc}} \approx |\lambda_0 - \Delta|$ . This quantity is nothing but the jump  $\mu_+ - \mu_-$  of the chemical potential in going from electron- to hole-doped systems and vanishes at the MCTI transition. We shall briefly comment on that in Sec. VI. Notice that near the insulating regime  $\omega_{\text{exc}} \approx |\lambda_0 - \Delta|$  is larger or smaller than the interband quasiparticle gap  $\Delta$  (i.e., the CT mode has antibound or bound character), depending on  $\lambda_0 - 2\Delta$  being larger or smaller than zero. Generally the CT mode is an anti-bound mode for large values of the bare CT gap at positive doping, while it is a bound mode at negative doping and near the MCTI transition.

At a given  $\lambda_0 - \Delta$ ,  $V$  decreases  $\omega_{\text{exc}}^2$  by a term  $-8V\lambda_0 r_0^2$ , which, being proportional to  $r_0^2$ , is quite small at small doping above the Brinkman-Rice (BR) point. The important point to make here is that in the phase diagram of Fig. 3,  $\lambda_0 - \Delta \approx \omega_{\text{exc}}$  is strictly positive at the intersections of the curves  $\chi_{\text{CT}} = \chi = \infty$  with the  $\delta = 0$  axis where  $r_0^2$  vanishes. More generally, all along the upper branch of the critical curve  $\chi_{\text{CT}} = \chi = \infty$  in the  $\delta - \Delta_0$  phase diagram  $\omega_{\text{exc}}$  is a large positive quantity (of the order of  $\lambda_0$ ) indicating that the CTI is not due to the softening of the CT mode. Numerical inspection of Eq. (27) shows that this is a general feature of the CTI, the lowest (nevertheless positive) values of  $\omega_{\text{exc}}$  at the CTI being attained in the lower branch of the CTI in the  $\delta - \Delta_0$  plane.

That no naive direct correlation exists between  $\omega_{\text{exc}} = 0$  and the CTI is strengthened by the observation that in the present strong-coupling framework  $\omega_{\text{exc}} (= \mu_+ - \mu_-$  at  $r_0 = 0$ ) does, in fact, vanish at the MCTI transition even in the case  $V = 0$ , where no CTI is present.

The lack of softening of the CT mode at the CTI is not, however, a peculiarity of the strong-coupling approach. As demonstrated in the preceding paper,  $\omega_{\text{exc}} \neq 0$  at the

CTI in the weak-coupling approach for moderate values of the copper-copper repulsion. In the weak-coupling analysis  $\omega_{\text{exc}}$  at the CTI is nevertheless quite small and it is difficult to resolve its difference from zero by a pure numerical analysis of the random-phase approximation (RPA) equations.

Equation (30) describes the CT mode in the dynamical limit when no coupling to the conserved field  $n_d(q) + n_p(q)$  is present. To go beyond this limit, and, in particular, to connect with instabilities that we have detected in the statistical limit, requires the generalization of the above analysis at finite momenta. This is carried out in a subsequent section along the lines of the weak-coupling analysis presented in the preceding paper. However, it is quite instructive from a physical point of view to perform first this generalization in the context of a Landau Fermi-liquid description.

#### IV. THE LANDAU FERMI-LIQUID PARAMETERS

Within our  $1/N$  expansion the system is a Fermi liquid as long as  $r_0$  has a finite value. The singlet interaction amplitude between quasiparticles with momenta  $k + q/2$  and  $k' - q/2$ , exchanging energy  $\omega$  and momentum  $q$ , is given by Eq. (20). By taking suitable limits we can evaluate the standard Landau amplitudes

$$\Gamma_\omega(k, k') = - \lim_{\omega \rightarrow 0} \lim_{q \rightarrow 0} \tilde{\Lambda}_{11}^\mu(k', -q) D^{\mu\nu}(q, \omega) \tilde{\Lambda}_{11}^\nu(k, q).$$

Notice that  $\Gamma_\omega(k, k')$  would depend on  $k$  and  $k'$  only via  $\gamma_k$  and  $\gamma_{k'}$  [see Eq. (16) for the vertices]. Therefore, by taking the quasiparticles at the Fermi surface (where  $\gamma_k = \text{const} = \gamma_F$ ), only the “zeroth” harmonic would be nonzero and given by

$$\Gamma_\omega = - \lim_{\omega \rightarrow 0} \lim_{q \rightarrow 0} \tilde{\Lambda}_{11}^\mu(k_F, -q) D^{\mu\nu}(q, \omega) \tilde{\Lambda}_{11}^\nu(k_F, q). \quad (33)$$

More explicitly we write  $\Gamma_\omega = \lim_{\omega \rightarrow 0} \Gamma(\omega)$ , where

$$\Gamma(\omega) = - \frac{1}{2Nr_0^2} \begin{pmatrix} \frac{R_{k_F}^2 - \Delta^2}{2R_{k_F}} \\ i \frac{R_{k_F} + \Delta}{2R_{k_F}} \\ \frac{\Delta}{R_{k_F}} \\ i \end{pmatrix} \begin{pmatrix} a & -i - ia(\Delta - \lambda_0) & 4r_0 Va & 0 \\ -i - ia(\Delta - \lambda_0) & \lambda_0 - (\Delta - \lambda_0)^2 a & -4ir_0^2 V(\Delta - \lambda_0)a & 0 \\ 4r_0 Va & -4ir_0^2 V(\Delta - \lambda_0)a & 2r_0^2 V(1 + 8r_0^2 Va) & 0 \\ 0 & 0 & 0 & 2r_0^2 V \end{pmatrix} \begin{pmatrix} \frac{R_{k_F}^2 - \Delta^2}{2R_{k_F}} \\ i \frac{R_{k_F} + \Delta}{2R_{k_F}} \\ \frac{\Delta}{R_{k_F}} \\ i \end{pmatrix} \quad (34)$$

with

$$a \equiv a(\omega) \equiv I(\omega) [1 - (2\Delta - \lambda_0 + 8r_0^2 V)I(\omega)]^{-1}.$$

The amplitude  $\Gamma_\omega$  sums the bare interactions and the interband processes only, the intraband bubbles being zero due to the  $q = 0$  limit first performed at finite frequency (again because of particle conservation).

The intraband screening processes can then be included by considering the opposite static limit of the scattering amplitude

$$\Gamma_q = - \lim_{q \rightarrow 0} \lim_{\omega \rightarrow 0} \tilde{\Lambda}_{11}^\mu(k_F, -q) D^{\mu\nu}(q, \omega) \tilde{\Lambda}_{11}^\nu(k_F, q). \quad (35)$$

The usual relation holds

$$\Gamma_q = \frac{\Gamma_\omega}{1 + NN_0\Gamma_\omega} = \frac{\Gamma_\omega}{1 + F_0^s}, \quad (36)$$

$N_0$  being the density of states per spin at the Fermi level and with the identification  $F_0^s = NN_0\Gamma_\omega$  leading to the standard definition of the  $F_0^s$  Landau parameter.

The static compressibility per unit spin  $\chi$  can then be written as

$$\begin{aligned} \chi &\equiv \chi(q \rightarrow 0, \omega = 0) \\ &= N_0(1 - NN_0\Gamma_q) = N_0(1 + F_0^s)^{-1}. \end{aligned} \quad (37)$$

The instability present in our model, i.e., the CTI, can now be interpreted in terms of Landau Fermi-liquid quantities. In particular, whereas the condition  $NN_0\Gamma_\omega > 0$  establishes the existence of a propagating zero-sound mode,<sup>20</sup> when  $0 > NN_0\Gamma_\omega > -1$  the zero-sound mode is in the particle-hole continuum and gets damped. Finally the instability is reached when

$NN_0\Gamma_\omega = -1$  leading to a divergent  $\Gamma_q$  [see Eq. (36)] and, consequently, to a diverging  $\chi$ . The zero sound gets overdamped. Being coupled to  $\chi$ ,  $\chi_{CT}$  diverges as well.

In the absence of  $V$  the condition  $F_0^s = -1$  is never reached. In fact, at  $V=0$ , the only singular point is at the MIT, where  $\omega_{exc}=0$ , with, however,  $\Gamma_\omega$  diverging to  $+\infty$ .<sup>10</sup> The compressibility goes to zero at the MCTI transition staying positive everywhere else. In the presence of  $V$  the interband processes generate a sizable effective attraction between the quasiparticles at the Fermi surface leading to a negative  $\Gamma_\omega$  and eventually  $F_0^s = NN_0\Gamma_\omega$  becomes minus unity by increasing  $V$ . In order to gain insight on this point it is very instructive to approach the calculation of  $\Gamma(\omega)$  by separating in Eq. (34) the  $\omega$ -dependent part

$$\Gamma(\omega) = \Gamma_0 + \Gamma_1 a(\omega), \quad (38)$$

where

$$\begin{aligned} N\Gamma_0 &= \frac{1}{2r_0^2} u_F^4 (\lambda_0 + 2R_{k_F} - 2\Delta) + 4Vu_F^2 v_F^2 \\ &= \frac{1}{8r_0^2} \left[ 1 + \frac{\Delta}{R_{k_F}} \right]^2 (\lambda_0 + 2R_{k_F} - 2\Delta) + V \left[ 1 - \frac{\Delta^2}{R_{k_F}^2} \right], \\ N\Gamma_1 &= -\frac{1}{2r_0^2} u_F^4 (\lambda_0 + R_{k_F} - 2\Delta)^2 + 4Vu_F^2 (u_F^2 - v_F^2) (\lambda_0 + R_{k_F} - 2\Delta) - 8r_0^2 V^2 (u_F^2 - v_F^2)^2 \\ &= -\left[ \frac{1}{\sqrt{2}r_0} u_F^2 (\lambda_0 + R_{k_F} - 2\Delta) - 2\sqrt{2}r_0 V (u_F^2 - v_F^2) \right]^2 \\ &= -\frac{r_0^2}{2} \left[ \frac{1}{2r_0^2} \left[ 1 + \frac{\Delta}{R_{k_F}} \right] (\lambda_0 + R_{k_F} - 2\Delta) - 4V \frac{\Delta}{R_{k_F}} \right]^2. \end{aligned}$$

Equation (38) can be written in a more physically transparent form using Eqs. (25) and (34), which identify  $a(\omega)$  in terms of  $\chi_{CT}(0, \omega)$ ,  $2r_0^2 a(\omega) = \chi_{CT}(0, \omega)$ . Defining  $g^2 = -N\Gamma_1 / (8r_0^2)$ , we write

$$\Gamma(\omega) = \frac{1}{N} \Gamma_0 - \left[ \frac{1}{N} g \right]^2 [N\chi_{CT}(0, \omega)]. \quad (39)$$

$(1/N)\Gamma_0$  is the bare, frequency-independent repulsion between quasiparticles. The second term in the rhs  $-[(1/N)g]^2 [N\chi_{CT}(0, \omega)]$ , is the dynamical attraction mediated by the CT mode (there are  $N$  equivalent CT modes).  $(1/N)g$  is the coupling between the quasiparticles at the Fermi surface and the CT mode.

$V$  drives  $\Gamma(\omega)$  negative because it reduces  $\omega_{exc}$ , Eq. (32), thus enhancing  $\chi_{CT}(0, \omega)$ . However, provided  $g^2$  is finite and positive, from Eq. (39) it is evident that the instability condition  $NN_0\Gamma_\omega = -1$  is always reached before the system meets the softening condition  $\omega_{exc}=0$  at which  $\chi_{CT}(0, \omega_{exc})$  diverges. This last feature is shared by both the weak- and strong-coupling descriptions of the CTI.

To analyze the specific features of the strong-coupling

limit it is convenient to consider the small- $r_0$  expansion of Eq. (38).

We obtain

$$\begin{aligned} N\Gamma_0 &= \frac{\lambda_0}{2r_0^2} + 4t_{pd}^2 \lambda_0 \gamma_F \left[ \frac{2}{\Delta \lambda_0} - \frac{1}{\Delta^2} \right], \\ N\Gamma_1 &= -8r_0^2 g^2 \approx -\frac{1}{2r_0^2} (\lambda_0 - \Delta)^2 + \frac{4t_{pd}^2 \gamma_F^2}{\Delta^2} (\lambda_0 - \Delta)^2 \\ &\quad + 2(\lambda_0 - \Delta)(2V - 4t_{pd}^2 \gamma_F^2), \\ a(\omega) &= \lambda_0 \frac{(1 - \alpha r_0^2)}{(\lambda_0 - \Delta)^2 + r_0^2 [\alpha(2\Delta - \lambda_0) - 8V] \lambda_0 - \omega^2}, \end{aligned}$$

with  $\alpha$  given by Eq. (31). We see that, near the insulating regime, for  $\delta$  (and  $r_0$ ) going to zero, all the interactions diverge reflecting the strong-coupling nature of the system. However, the leading  $1/r_0^2$  singularities cancel, leaving a finite  $\Gamma_\omega$  in the limit  $r_0 \rightarrow 0$  (as already mentioned, the BR point is exceptional in this regard). The main effect of  $V$  is to shift the denominator of  $a$  (i.e.,  $\omega_{exc}$ ) by the small amount  $-8r_0^2 V \lambda_0$ . Nevertheless, this effect

can be dramatic because the coupling  $g$  (or  $-\Gamma_1$ ) is diverging at the same time. This leads to a finite  $[O(r_0^0)]$  negative contribution to  $\Gamma_\omega$  proportional to  $V$ , which can overcome its positive value at  $V=0$ . The total expression of  $\Gamma_\omega$  in the limit  $r_0, \delta \rightarrow 0$ , is

$$N\Gamma_\omega = \frac{4\lambda_0}{\omega_{\text{exc}}^2} \left[ 2t_{pd}^2 \left[ \frac{\gamma_4}{\gamma_2} - \left[ 1 - \frac{\Delta^2}{4t_{pd}^2\gamma_2} \right] \right] - \Delta V \right]$$

with  $\omega_{\text{exc}}^2 = (\lambda_0 - \Delta)^2$ .  $\Gamma_\omega$  becomes negative for

$$V > \frac{2t_{pd}^2}{\Delta} \left[ \frac{\gamma_4}{\gamma_2} - 1 + \frac{\Delta^2}{4t_{pd}^2\gamma_2} \right] \equiv h(\Delta). \quad (40)$$

At the same time, since  $N_0$  ( $\sim 1/r_0^2$ ) diverges, the condition in Eq. (40) is the same condition for the instability to occur.

In the region we are considering here,  $\Delta$ , whose specific value depends on the various bare parameters of our model, ranges from zero to  $\Delta_0^c/2 = 2t_{pd}\gamma_2^{1/2} \approx 1.65t_{pd}$ , this latter value being reached at the BR point. In this range of  $\Delta$ 's the function  $h(\Delta)$  has a minimum at  $\Delta_{\text{min}} = 2t_{pd}\sqrt{\gamma_4 - \gamma_2}$  and

$$h(\Delta_{\text{min}}) = \frac{2t_{pd}}{\gamma_2} \sqrt{\gamma_4 - \gamma_2} \approx 1.63t_{pd}.$$

This last value is the minimum value  $V = V_{\text{min}}$  required for the system to be unstable. We have then obtained the expression already reported in the previous section.

The value

$$V^* = h\left(\frac{\Delta_0^c}{2}\right) = \frac{t_{pd}\gamma_4}{\gamma_2^{3/2}} \approx 1.76t_{pd}$$

is the value at which the MCTI transition becomes first order and the self-consistency equations (10)–(14) start to develop two solutions.

For  $V_{\text{min}} < V < V^*$  two instability points, with  $F_0^s = -1$ , are met along the line  $\delta=0$  in the  $\delta-\Delta_0$  plane. By generalizing the above analysis at finite  $\delta$  one recovers the picture given in Sec. II A. In particular, we could identify the curve  $\chi = \chi_{\text{CT}} = \infty$  which signals the presence of a phase-separation region to be determined by the Maxwell construction.

In the presence of the exchange term  $V_2$ , the expression for  $\Gamma_\omega$  has the same structure as in Eq. (38) with

$$\begin{aligned} N\Gamma_0 &= \frac{1}{2r_0^2} u_F^4 \left[ \lambda_0 + (2R_{k_F} - 2\Delta) \left[ \frac{1}{1+y} - \frac{v_F^2}{(1+y)^2} \frac{R_{k_F} V_2}{4t_{pd}^2} \right] \right] + 4V u_F^2 v_F^2, \\ N\Gamma_1 &= -\frac{1}{2r_0^2} u_F^4 \left[ [\lambda_0(1+y) + R_{k_F} - 2\Delta]^2 + 2(R_{k_F} - \Delta) \left[ y\Delta - \frac{y}{1+y} \frac{\Delta^2}{\lambda_0} \right] \right] \\ &\quad - \frac{1}{2r_0^2} u_F^4 \left[ \frac{(R_{k_F} - \Delta)^2}{\lambda_0} \frac{y}{1+y} \left[ 2 + \frac{y}{1+y} \frac{\Delta}{\lambda_0} \right] \right] \\ &\quad + 4V u_F^2 (u_F^2 - v_F^2) \left[ \lambda_0(1+y)^2 + R_{k_F} \left[ 1 + y + y \frac{\Delta}{\lambda_0} \right] - 2\Delta \left[ 1 + y + y \frac{\Delta}{2\lambda_0} \right] \right] - 8r_0^2 V^2 (u_F^2 - v_F^2)^2 (1+y)^2, \end{aligned}$$

where  $y = \lambda_0 V_2 / 4t_{pd}^2$  and in the expressions for  $u_F$ ,  $v_F$ , and  $R_{k_F}$  one has to replace  $t_{pd}$  with  $t_{pd}(1+y)$ . At the same time  $a_\omega \equiv a(\omega \rightarrow 0)$  takes the form

$$a_\omega \equiv I_\omega \left[ 1 - (1+y)^2 (\Delta - \lambda_0 + 8r_0^2 V) I_\omega + \Delta \left[ 1 + \frac{\Delta}{\lambda_0} y - y^2 \right] I_\omega \right]^{-1}.$$

By extending to the case  $V_2 \neq 0$ , the analysis performed for  $V_2 = 0$  in the limit  $r_0, \delta \rightarrow 0$ , we obtain the expression for  $\Gamma_\omega$

$$N\Gamma_\omega = \frac{4\lambda_0\Delta}{\omega_{\text{exc}}^2(1+y)} [h(\Delta, V_2) - V]$$

with  $\omega_{\text{exc}}^2 = [\lambda_0 - \Delta/(1+y)]^2$ .  $\Gamma_\omega$  becomes negative for

$$V > h(\Delta, V_2) \equiv \frac{2t_{pd}^2}{\Delta} \left[ \frac{\gamma_4}{\gamma_2} (1+y)^2 - (1+y) + \frac{\Delta^2}{4t_{pd}^2\gamma_2(1+y)} \right]. \quad (41)$$

Similarly to the previous case with  $V_2 = 0$ , the above equation allows one to determine the conditions for the occurrence of the instability. Specifically, for  $V_2 = 0.5V$  we find that on the  $\delta=0$  line  $V_{\text{min}} = V^*$ .

## V. DYNAMICAL ANALYSIS AT FINITE $q$

In this section we report the numerical evaluation of the dynamical correlation functions at finite  $q$  in the strong-coupling limit. We also analyze the frequency dependence of the effective interaction the Cooper channel. The results confirm and conclude the analysis presented in the previous section on the role of  $V$  in the dynamics of the three-band Hubbard model at  $U_d = \infty$ .

In Figs. 7(a) and 7(b) we show the spectral density of the total density-density correlation function  $\chi(q, \omega)$  with parameters of  $V=1.75t_{pd}$ ,  $\varepsilon_p^0 - \varepsilon_d^0 = 3.5t_{pd}$ , and  $\delta=0.3$ . This set of parameter, for which  $s$ -wave and  $d$ -wave pairing was obtained<sup>1</sup> is outside but close to the upper boundary of the phase separation. The peak, which disperses just above the intraband particle-hole continuum, is the zero-sound mode. At small momentum it is damped into the particle-hole continuum, signaling a negative value of  $F_0^s$ , while it becomes a well-defined collective mode separated from the particle-hole continuum at larger momenta. This is contrasting with a homogeneous Fermi liquid with a parabolic band, where the zero sound is usually well defined at low momentum and disappears by Landau damping for high momentum. This is because of the tight-binding band structure of the model. At high frequency ( $\omega/t_{pd} \sim 3.7$ ), a collective mode of a strong oscillator strength exists. This is the mode which corresponds to the CT excitonic mode in the weak-coupling limit. Here the CT fluctuation makes an antibound state above the interband gap rather than a bound state below the gap as in the weak-coupling case [compare the discussion after Eq. (28)]. The characteristic frequency of this antibound mode is given by Eq. (32) in the  $q \rightarrow 0$  limit. For the set of parameters considered here the first term of Eq. (32) is roughly the bare CT gap<sup>8</sup> and the second term reduces it by the attraction of  $V$  in the CT channel

$$\omega_{\text{exc}}^2 \approx (\Delta - \lambda_0)^2 - 8r_0^2 \lambda_0 V. \quad (42)$$

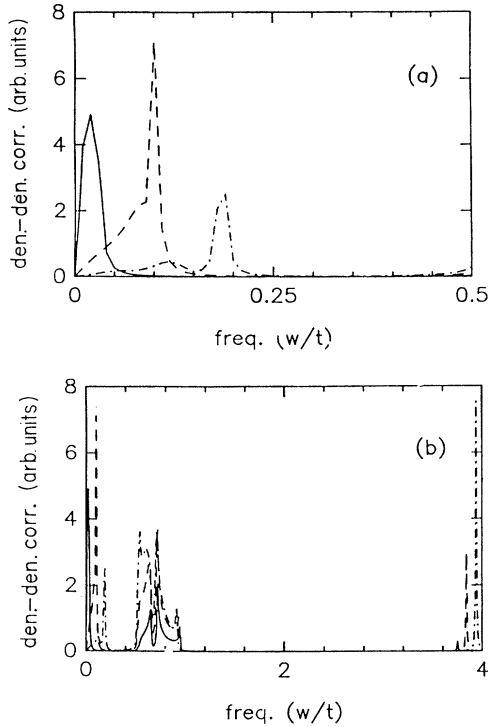


FIG. 7. (a) The spectral density of the total density-density correlation function with  $\varepsilon_p^0 - \varepsilon_d^0 = 3.5$ ,  $V = 1.75$ , and  $\delta = 0.3$ , with the momenta  $q = (2/30\pi, 2/30\pi)$  (solid line),  $q = (6.30\pi, 6/30\pi)$  (dashed line), and  $q = (10/30\pi, 10/30\pi)$  (dash-dotted line). (b) Plot of (a) for a larger frequency range.

The prefactor of  $V$  in the second term is about 0.3. Since this high-energy antibound mode carries a dominant oscillator strength, it will control the dynamics at the high energy, while zero sound provides the dynamic structure for the energy range less than the conduction bandwidth ( $\sim 0.4t_{pd}$ ).

Figures 8(a) and 8(b) are the spectral density of the CT susceptibility with the same parameters as in Figs. 7(a) and 7(b). It shows the same behavior as the total density-density correlation function except the peak strength.

To see the effect of  $V$ , we turn off  $V$  in Figs. 9(a) and 9(b). Now the damping of the zero sound at small momenta is substantially reduced and the peak disperses much faster. The antibound mode peak is also moved towards higher frequency showing the effect of  $V$ . From these results it is clear that zero-sound mode gets damped by the attraction mediated by the high-energy antibound mode; the lower the frequency of the antibound mode is, the stronger the attraction is. Notice that the zero sound easily gets damped even with a weak attraction when the coherent conduction bandwidth is renormalized by a factor  $\delta$ , since  $F_0^s = N_0 \Gamma_\omega$ , with  $N_0 \sim 1/\delta$ . When the condition  $F_0^s = -1$  is eventually met this overdamped sound mode is the direct cause of the phase separation. Near the phase-separation boundary we expect  $s$ -wave pairing to be promoted by the same attractive interaction leading to  $F_0^s \approx -1$ .<sup>1,2</sup> In fact,  $\chi \sim 1/(1+F_0^s)$  is large near the phase separation, therefore  $-1 < F_0^s < 0$  and it provides attractive interaction in the  $s$ -wave channel. (This argu-

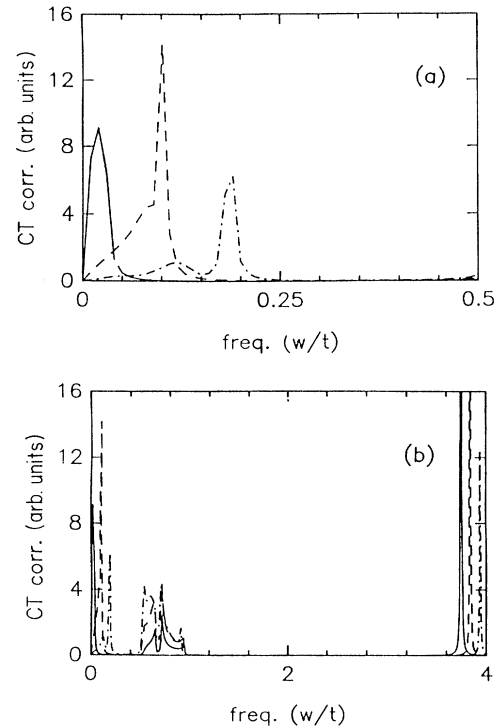


FIG. 8. (a) The spectral density of the CT susceptibility for a small frequency range with the same parameters and momenta as in Fig. 7. (b) Plot of (a) for a larger frequency range.

ment is qualitatively correct for not too small doping when the Fermi surface is quite isotropic.)

In Fig. 10(a), with same set of parameters as in Figs. 7(a) and 7(b), we show  $\Gamma(k, k'; \omega)$  for different sets of  $k$  and  $k'$  on the Fermi surface. For the small momentum exchange ( $|k - k'| \leq 1$ ), the effective interactions  $\Gamma(k, k'; \omega)$  are attractive at low frequency just as in the weak-coupling results. This agrees with the presence of a damped zero sound. However, there is not interesting structure in the range of the interband continuum ( $0.5 \leq \omega/t_{pd} \leq 1$ ) because the dynamics of this frequency region is already dominated by the antibound mode at higher energy, which carries a strong oscillator strength [see Eq. (39)].

In Fig. 10(b), with  $V=0$ ,  $\Gamma(k, k'; \omega)$  is repulsive at low frequency because the antibound mode is at relatively higher energy and, as discussed in the previous section, the repulsion prevails in the screening process at  $V=0$ . In Fig. 10(c), we shut off the intraband process, therefore there is no zero-sound contribution and  $\Gamma(k, k'; \omega)$  is now mediated by the high-energy antibound mode only. The plot is almost the same as Fig. 10(a) except the low-energy structure.

The numerical results of this section together with the analytical results of Secs. II B and III allow one to draw the following summary of our findings in the dynamics of the three-band model in the  $U = \infty$  limit. Near the CTI at a moderately large bare CT gap (and small and intermediate doping), the CT mode has a higher energy with respect to the corresponding low-energy CT excitonic

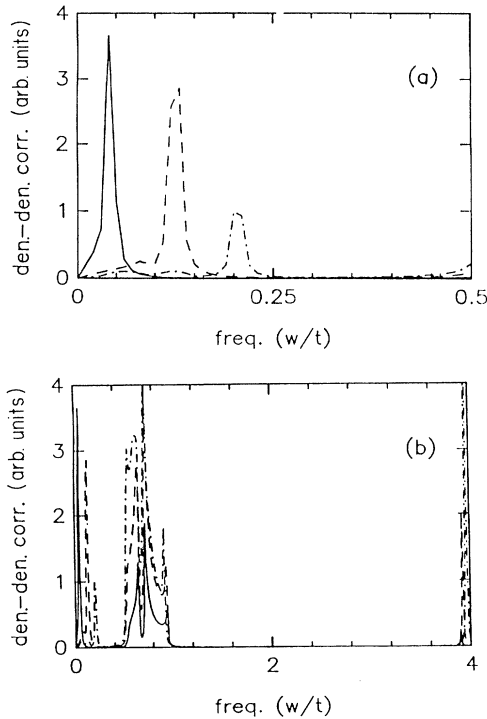


FIG. 9. (a) The spectral density of the total density-density correlation function with the same parameters as in Fig. 7, except  $V=0$ . (b) Plot of (a) for a larger frequency range.

mode in the weak-coupling limit. Even when this mode has an antibound character, it carries a strong oscillator strength and it controls the dynamics of the energy range above the renormalized conduction bandwidth.

Moreover, the CT mode also strongly couples to the quasiparticles and strongly screens their large bare repulsion even at  $V=0$ . However, without  $V$ , the compressibility or the effective interaction in the static limit are never negative. Now with a finite  $V$  of the order of  $t_{pd}$ , the energy of the CT mode is slightly reduced but this softening generates an attractive interaction which is strong enough to drive a CTI and to make the effective Cooper interaction between the quasiparticles attractive. Regardless of its high energy, the strong collective mode

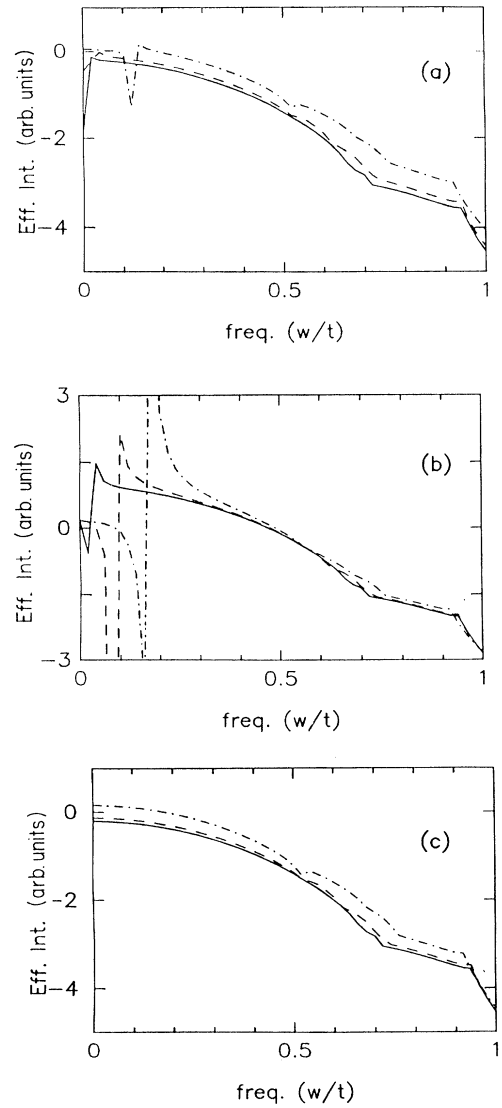


FIG. 10. The effective interaction in the Cooper channel  $\Gamma(k, k'; \omega)$  with  $\epsilon_p^0 - \epsilon_d^0 = 3.5$ ,  $\delta = 0.3$ , and (a)  $V = 1.75$ , (b)  $V = 0$ , and (c)  $V = 1.75$  and the intraband process shut off; all momenta  $k$  and  $k'$  are on the Fermi surface,  $k_y = k'_y$  and  $k_x - k'_x = 0.2, 0.6$ , and  $1.4$  for solid line, dashed line, and dash-dotted line, respectively.

mediates an attractive interaction for frequencies below its characteristic frequency  $\omega_{\text{exc}}$  once it strongly couples to the quasiparticles. However, if the system had only repulsive couplings in every channel, it would be very hard to have the effective interaction be attractive in the  $q \rightarrow 0$  and  $\omega \rightarrow 0$  limits, even when all dynamic screenings and the local field effects are included. Our case with  $V=0$  shows this difficulty. However, we have a more favorable condition for the pairing because  $V$  acts as an attraction in the CT channel. This effect can shift the already subtle balance towards a negative  $\Gamma(k, k'; \omega=0)$  and eventually a negative compressibility. Thus, the softening of the antibound mode by  $V$  is just a dynamical realization of this subtle balance between the repulsion and the attraction.

Therefore, a low-energy collective mode is not necessary in order to have the instabilities and the superconducting pairings in the strong-coupling regime. The strong correlation effect substantially modifies the character of the charge-transfer exciton physics, in comparison with the weak-coupling regime. However, as in the weak-coupling regime, the intersite Coulomb interaction  $V$  is crucial to finally drive the instabilities and the attractive interaction in the Cooper channel. The strong correlation effect reduces the width of the quasiparticle band, making the system more vulnerable to the instabilities. The bound (excitonic) collective mode of the small- $U$  limit becomes a higher-energy collective mode (possibly an antibound mode above the interband gap), with large oscillator strength.

## VI. CONCLUSIONS

In this paper we focused our analysis on the charge collective modes in the three-band Hubbard model. We studied both the weak-coupling and the strong-coupling regimes. In both cases, when  $V \sim t_{pd}$ , the charge degrees of freedom affect the low-energy properties leading to a CTI (and phase separation) and a pairing instability. An issue of the present work has been to elucidate the role of the collective modes in these instabilities and to identify the similarities and the differences between the strong- and the weak-coupling limits. In both cases the CTI is characterized by the divergency of  $\chi$  and  $\chi_{\text{CT}}$ , and leads to the violation of the Landau stability criterion  $F_0^s > -1$  and produces an overdamped zero-sound mode. The attraction leading to  $F_0^s = -1$  is mediated by the CT mode which, however, has a low energy at the CTI in the weak-coupling limit and a high energy in the strong-coupling limit. In this latter case the strong coupling of the CT mode to the quasiparticles overcompensates for the high energy of the mode.

In the absence of long-range Coulomb interactions we conclude that the excitonic mechanism for pairing, which works at a small value of  $U_d$ , works in the strong-coupling limit as well. However, the region of momenta in which the effective interaction is attractive is substantially reduced (and is pushed towards small momentum transfer), with respect to the corresponding weak-coupling result. A main problem concerns the location of the pairing instability, which occurs near (but outside)

the phase-separation region. This criterion restricts the optimal location in the parameter space at the boundary of the stability region, possibly near the critical points for phase separation, where the phase-separation boundary is very close to the point where  $\chi$  and  $\chi_{\text{CT}}$  diverge.

On the other hand, the presence of a superconducting phase will change the phase-separation boundary derived for the normal phases and we expect a reduction of the phase-separated region in favor of the superconducting phase.<sup>21</sup>

In the strong-coupling limit the effective interaction in the Cooper channel is attractive at small  $q$  in a range of energy larger than the renormalized bandwidth. As long as the small- $q$  region ( $|q| \leq 1$ ) is dominant for the pairing, the energy scale below which pairing occurs is set by  $\epsilon_F$  ( $\approx 0.4$  eV) measured from the bottom of the occupied band. In view of the value of the Cooper coupling in the  $s$ -wave channel,  $\lambda_s \approx 0.5$ ,<sup>1,2</sup> a large  $T_c$  (a few tenths of  $\epsilon_F$ ) can be obtained.

Notice, however, that small variations in the parameter space lead to a strong reduction of  $\lambda$ , mainly because  $\Gamma(k, k', \omega)$  strongly depends on  $q = k - k'$ . This is because, in the strong-coupling limit, the screening of the large bare repulsion is only effective at not too large  $q$ 's.

The above comments refer to the short-range model Eq. (5). Additional remarks are in order if we include long-range forces. An important effect of the long-range Coulomb forces is to prevent the occurrence of phase separation when the ions are immobile. At small  $q$ 's the zero sound is substituted by a plasmon mode which experimentally has a three-dimensional (3D) character and energy of the order of  $\approx 1$  eV.<sup>22</sup> Inside the region of negative compressibility for the short-range model, the competition between phase-separation and long-range forces would result in an incommensurate charge-density-wave (CDW) phase or in the formation of droplets of hole-rich and hole-poor phases. The specific sizes of possible incommensurate CDW's or droplets, the effects of the coupling between the CT mode and the plasmon mode, and the anisotropy of the modes are interesting topics which will deserve a future analysis.<sup>23</sup>

As far as pairing is concerned the inclusion of long-range forces results in the old problem of competition between Coulomb repulsion and attraction from a high-energy mode. The analysis of Ref. 24 suggests that, in this case, the inclusion of self-energy and vertex corrections leads to a strong reduction of  $T_c$  with respect to the naive mean-field estimates neglecting Coulomb long-range forces. However, a quantitative estimate of this reduction is quite difficult since it requires detailed knowledge of  $V_{\text{eff}}(q, \omega)$  and a full solution of an equation of the Eliashberg type. This analysis is beyond the scope of this work which intended to analyze the stability of excitonic pairing in the three-band Hubbard model with respect to the large local repulsion.

Finally, we comment on the role of the CT mode and of the zero-sound mode near the MCTI transition. The analysis of the dynamics of the boson propagators has shown the presence of a collective interband mode, the CT mode, characterized by a frequency which we identified with  $\omega_{\text{exc}}$  to stress its connection with the exci-

tonic resonance discussed in the weak-coupling framework.  $\omega_{\text{exc}}$  is finite at the CTI, while it is zero at the MCTI transition whenever this transition is second order (i.e., for  $V < V^*$ ). In fact, we were pointing out that near the insulating regime (i.e., at small doping and  $\Delta_H > \Delta_0^c + V$ ),  $\omega_{\text{exc}}$  equals the jump in the chemical potential  $\mu_+ - \mu_-$ . An important observation is that the CT mode is present irrespective of the presence of  $V$  and, for small  $r_0$ , its natural strong-coupling interpretation is in terms of the dynamics of the MCTI transition (gap mode). This issue has been recently addressed by Castellani *et al.*<sup>25</sup> The presence of this mode even in the metallic region ( $\Delta_H < \Delta_0^c + V$ ) can be interpreted as a precursor effect of the MCTI transition. Both the single-particle gap and the optical gap are controlled by  $\omega_{\text{exc}}$ , which vanishes at the MCTI transition. The softening of a collective mode near the metal-insulator transition can be relevant in developing non-Fermi-liquid (or almost non-Fermi-liquid) properties near half filling. In the presence

of a sizable  $V$ , the physics of the MCTI transition is moved at finite doping in a region, which, however, is unaccessible because of phase separation. If long-range forces stabilize the system to make it possible to reach  $\omega_{\text{exc}} \approx 0$  for  $V > V^*$ , the low-energy CT mode could be of relevance for marginal behavior at finite doping possibly via strong polaronic effects.

#### ACKNOWLEDGMENTS

G.K. was supported by the NSF under Grant No. DMR 89-15895. We acknowledge hospitality of the Institute for Scientific Interchange Foundation of Torino. M.G. acknowledges financial support from Progetto SAT of the "Consorzio Interuniversitario di Fisica della Materia" (INFM). C.C., M.G., and R.R. were supported by the European Economic Community under Contract No. SC1\* 0222-C(EDB). We also thank A. R. Ruckenstein for communicating unpublished results to us.

\*Present address: Max-Planck-Institute für Festkörperforschung, Heisenbergstrasse 1, Postfach 800665, D-7000 Stuttgart 80, Federal Republic of Germany.

<sup>1</sup>M. Grilli, R. Raimondi, C. Castellani, C. Di Castro, and G. Kotliar, Phys. Rev. Lett. **67**, 259 (1991).

<sup>2</sup>M. Grilli, R. Raimondi, C. Castellani, C. Di Castro, and G. Kotliar, Int. J. Mod. Phys. B **5**, 309 (1991).

<sup>3</sup>The weak-coupling approach can, actually, give a metal-insulator transition, but at the price of breaking the spin symmetry by the introduction of spin long-range order. In this case the insulating behavior would be due to the magnetic correlations (Slater insulator) rather than to the Hubbard repulsion (CT insulator).

<sup>4</sup>Y. Bang, G. Kotliar, C. Castellani, M. Grilli, and R. Raimondi, Phys. Rev. B **43**, 13 724 (1991).

<sup>5</sup>S. E. Barnes, J. Phys. F **6**, 1375 (1976); P. Coleman, Phys. Rev. B **29**, 3035 (1984); N. Read and D. M. Newns, J. Phys. C **16**, 3273 (1983); N. Read, *ibid.* **18**, 2651 (1985); A. J. Millis and P. A. Lee, Phys. Rev. B **35**, 3394 (1987); G. Kotliar and A. R. Ruckenstein, Phys. Rev. Lett. **57**, 1362 (1986).

<sup>6</sup>Notice that the convention used in this paper slightly differs from the one of Refs. 1 and 2, where  $X$  and  $Y$  were coupled to the CT and to the total density of the cluster formed by a copper atom and the four surrounding oxygens.

<sup>7</sup>A. Houghton, N. Read, and H. Won, Phys. Rev. B **37**, 3782 (1988).

<sup>8</sup>G. Kotliar, P. A. Lee, and N. Read, Physica C **153-155**, 538 (1988).

<sup>9</sup>Since from now on  $V^*$  will indicate the value of  $V^*(\delta)$  at zero doping,  $V^* \equiv V^*(\delta = 0)$ .

<sup>10</sup>Y. Bang, C. Castellani, M. Grilli, G. Kotliar, R. Raimondi, and Z. Wang, Proceedings of the International Adriatico Conference on Strongly Correlated Electron Systems [Int. J. Mod. Phys. B **6**, 531 (1992)].

<sup>11</sup>J. D. Jorgensen, P. Lightfoot, Shiyong Pei, B. Dabrowski, D. R. Richards, and D. G. Hinks, *Third International Symposium on Superconductivity, Sendai, Japan, 1990* (Springer-Verlag, Tokyo, 1991).

<sup>12</sup>C. Castellani, M. Grilli, and G. Kotliar, Phys. Rev. B **43**, 8000 (1991).

<sup>13</sup>V. J. Emery, S. A. Kivelson, and H. Q. Lin, Phys. Rev. Lett. **64**, 475 (1990).

<sup>14</sup>However, a reliable Maxwell construction, which possibly includes both the magnetically driven and excitonically driven phase separations, would require the concomitant analysis of the  $V$  and  $J$  terms for a larger region of doping up to  $\delta \sim 0.12-0.3$ .

<sup>15</sup>P. B. Littlewood, C. M. Varma, and E. Abrahams, Phys. Rev. Lett. **63**, 2602 (1989).

<sup>16</sup>R. Putz, G. Dopf, B. Ehlers, L. Lilly, A. Muramatsu, and W. Hanke, Phys. Rev. B **41**, 853 (1990).

<sup>17</sup>Y. Bang, K. Quader, E. Abrahams, and P. B. Littlewood, Phys. Rev. B **42**, 4865 (1990).

<sup>18</sup>The specific features introduced by  $V_2$  do not modify qualitatively the results and are, therefore, immaterial in the present context (see Ref. 10).

<sup>19</sup> $-(2\Delta - \lambda_0 + 8r_0^2V)$  has the meaning of an effective interaction for the resonant interband particle-hole process and is derived from the bare exchange of the "ligand" boson combination  $\phi = \frac{1}{2}(i\lambda_0 + \Delta r) + X$ ,  $\langle \phi\phi \rangle_0 = (1/8r_0^2)(2\Delta - \lambda_0 + 8r_0^2V)$ .

<sup>20</sup>See, e.g., G. Baym and C. Pethick, in *The Physics of Liquid and Solid Helium*, edited by K. H. Bennemann and J. B. Ketterson (Wiley, New York, 1977).

<sup>21</sup>This is in analogy with the recent results for the Kondo-lattice model. N. Cancrini, S. Caprara, C. Castellani, C. Di Castro, M. Grilli, and R. Raimondi, Europhys. Lett. **14**, 597 (1991).

<sup>22</sup>N. Nücker, U. Eckern, J. Fink, and P. Müller, Phys. Rev. B **44**, 7155 (1991).

<sup>23</sup>Preliminary estimates, by comparing the electrostatic cost to the energy gain from charge segregation, give a typical drop-size of three or four lattice constants. The same values are obtained by the zero of the dielectric constant  $\epsilon = 1 + (4\pi e^2/\epsilon_0 q^2)\chi(q, \omega)$ .

<sup>24</sup>M. Grabowski and L. J. Sham, Phys. Rev. B **29**, 6132 (1984).

<sup>25</sup>C. Castellani, G. Kotliar, R. Raimondi, M. Grilli, Z. Wang, and M. Rozenberg, Phys. Rev. Lett. **69**, 2009 (1992).